Classification
*Physics Abstracts*
87.20C — 82.70K — 64.60C

# Phase transitions and shapes of two component membranes and vesicles I: strong segregation limit

Toshihiro Kawakatsu ([1,2]), David Andelman ([1,3]), Kyozi Kawasaki ([1,2]) and Takashi Taniguchi ([1])

([1]) Department of Physics, Kyushu University 33, Fukuoka 812, Japan
([2]) IFF Theorie III, Forschungszentrum Jülich, 5170 Jülich, Germany
([3]) School of Physics and Astronomy, Tel-Aviv University, Ramat Aviv 69978, Tel Aviv, Israel

*(Received 17 February 1993, accepted 13 April 1993)*

**Abstract** . — We investigate unilamellar membranes and vesicles composed of an A/B mixture of partially miscible amphiphiles. Assuming a simple bilinear coupling between relative composition and local curvature, and in the strong segregation limit of the A/B mixture, we show for unilamellar open-shape membranes that the competition between surface tension and curvature results in a phase with a selected periodicity (modulated phase) both in the shape and in the A/B composition. The limits of large and small surface tension are discussed separately. These findings extend previous results obtained close to the A/B critical point (shallow quench). For the same limit of strong segregation, we also investigate the coupling between the separation of the system into A and B domains, and the overall shape of closed–shape vesicles. For cylindrical vesicles of fixed overall area (or equivalently vesicles embedded in a two–dimensional space), equilibrium shapes and phase diagrams are obtained. We also consider the effect of an added pressure difference (osmotic pressure) across the vesicle. The results are extended to axial symmetric vesicles embedded in a three–dimensional space.

## 1. Introduction.

Physics of supermolecular structures in mesoscopic scales has been an active area of theoretical and experimental research in recent years [1-3]. Membranes and vesicles are well-known examples of self-assembled supermolecular structures of amphiphilic molecules, which are formed when the amphiphilic molecules are dissolved in water. The membrane is composed of a bilayer of amphiphilic molecules having their head-group pointing towards the water, and the vesicle is just a closed–form object composed of such a bilayer membrane. Since Helfrich's pioneering work on the membrane shape deformation [4], a large number of theoretical works have been published [1-3, 5-9], most of which is focused on shape deformations of structureless membranes and vesicles.

However, it has recently been recognized that a membrane shape deformation can also be induced by a change in the internal degrees of freedom within the membrane. For example, an order-disorder transition of the hydrocarbon chain conformation, or an inplane phase separation of two-component amphiphilic mixtures [10-20]. Shape deformations of two-component membranes coupled to an inplane phase separation were investigated for the weak–segregation limit, where the two amphiphiles are only weakly immiscible with each other [12], and in the strong–segregation limit, where the two amphiphiles are strongly immiscible and the membrane is divided into domains separated by sharp domain walls [13]. Similar coupling was used to study two-component closed–form vesicles in both strong and weak segregation limits [13, 14]. These works are closely related to some other recent works [16-19]. Seifert investigated shape deformations of a two-component membrane in its one-phase region (above the critical temperature) and showed that the system can be mapped to a one-component membrane with renormalized bending elasticity moduli [16]. Lipowsky discussed the budding of a membrane in connection with a phase separation within the membrane and showed that such a phase separation can cause the budding [17], which are extended by Jülicher and Lipowsky to a closed form vesicle [18]. Very recently, Onuki explored the dynamics of two-component membranes and vesicles and proposed a dynamical model of a phase separation process on a membrane coupled to its shape deformation [19].

In this paper, we present a detailed study of shape deformations of two-component unilamellar membranes as well as closed-form vesicles undergoing an inplane phase separation and concentrating on the strong segregation limit. The other limit of weak segregation, will be presented in detail in the accompanying paper [20]. Our paper is organized as follows. In the next section, we study shape deformations of a unilamellar membrane. In section 3, we consider a single cylindrical vesicle of constant total membrane area, which can effectively be treated as a one-dimensional vesicle embedded in a two-dimensional space, and calculate the phase diagram of the shape deformations. The constraint on the membrane area turns out to have an important effect on closed-shaped vesicles in comparison with the case of the open membranes discussed in section 2. In section 4, the formalism is extended to two-dimensional uniaxial vesicles embedded in a three-dimensional space, and our conclusions are presented in section 5.

## 2. Unilamellar membranes.

In this section, we investigate undulations of an almost planar unilamellar membrane. Let us consider a model system of a single membrane (a single bilayer) immersed in a solution with an additional "internal" degree of freedom: the membrane is composed of two different species which have in general a miscibility curve for inplane phase separation. Possible examples are mixtures of surfactants (anionic, non-ionic or cationic), mixtures of phospholipids like phosphatidyl choline (PC) and phosphatidyl glycerol (PG), or mixtures of surfactant/lipids as are commonly used in reconstituted membranes [10].

The free energy of this system [12] is composed of three parts: $F = F_1 + F_2 + F_3$, where $F_1$ is the deformation free energy associated with shape changes, $F_2$ is the free energy of mixing associated with the inplane degrees of freedom, and $F_3$ is a coupling term (found on phenomenological grounds) which couples the local A/B composition with the local curvature.

Let us first discuss the shape free energy. Since we assume that the out-of-plane fluctuations about a mean flat plane are relatively of small magnitude and rather gradual in their wavelength, we can use the Monge representation to parametrize the surface by its height function above a reference plane, $z = h(x, y)$. The area element and curvature are expressed by the

lowest terms in a gradient expansion of $h$. We consider a membrane or rather an interface whose total area can be changed since the interface composed of amphiphiles is in contact with an amphiphile reservoir. The relevant energy terms in this case are the interfacial and the out-of-plan bending energies:

$$F_1 = \frac{1}{2}\sigma \int (\nabla h)^2 \, \mathrm{d}x \, \mathrm{d}y + \frac{1}{2}\kappa \int (\nabla^2 h)^2 \, \mathrm{d}x \, \mathrm{d}y \tag{2.1}$$

where $\sigma$ is the surface tension and $\kappa$ is the bending modulus. The second term expresses the so-called mean curvature elasticity [4]. More generally, a Gaussian curvature and a spontaneous curvature should also be included. However, for the almost planar unilamellar membrane under consideration, the Gaussian curvature gives only a constant contribution irrespective of the shape deformation according to the Gauss-Bonnet Theorem [21] and the spontaneous curvature contribution is written as a total derivative of some function, which can be re-expressed as boundary terms using the Gauss' Theorem and is expected to be negligible for the planar membrane case.

For the inplane degree of freedom, we choose a scalar field which is, for example, the relative composition of the two amphiphiles, $\varphi(x, y)$. We do not take into account the possibility of having two different order parameters, $\varphi_1$ and $\varphi_2$, for the "up" and "down" layers of the membrane. This type of partitioning has been investigated in detail by Safran and co-workers and offers a possible explanation of spontaneous vesiculation seen in experiments of surfactant mixtures [22]. In our case, the free energy of mixing can be written in terms of the scalar order parameter $\varphi$.

$$F_2 = \int \left[ \frac{b}{2}(\nabla \varphi)^2 + \frac{b^*}{2}(\nabla^2 \varphi)^2 + f(\varphi) - \mu \varphi \right] \mathrm{d}x \, \mathrm{d}y \tag{2.2}$$

where $b$ and $b^*$ are the "stiffness" coefficients in this gradient expansion and represent the resistance to local composition fluctuations of $\varphi$. The lateral (homogeneous) free energy of mixing is $f(\varphi)$ and the chemical potential coupled to the A/B composition is $\mu$.

The last term in the free energy is the coupling term $F_3$. On symmetry grounds, we write down the coupling term between $\varphi$ and even powers of the gradient of $h$:

$$F_3 = \Lambda \int \varphi(x, y) \nabla^2 h(x, y) \, \mathrm{d}x \, \mathrm{d}y + \Lambda^* \int \varphi(x, y) \nabla^4 h(x, y) \, \mathrm{d}x \, \mathrm{d}y \tag{2.3}$$

Where $\Lambda$ and $\Lambda^*$ are the composition – shape coupling constants. Since the results do not depend in a qualitative way on the higher-order terms in equations (2.2) and (2.3) we will set $b^* = 0$ and $\Lambda^* = 0$ in the following. The coupling terms introduced in equation (2.3) correspond to *asymmetric* membranes, since convex and concave regions of the membrane will prefer, say, high and low values of the relative concentration $\varphi$. This is possible if the membrane is a single monolayer at the interface of two different liquids. Another possibility is an induced asymmetry between the "up" and "down" layers of the bilayer-membrane due to a composition difference between these two layers.

Combining equations (2.1-2.3) defines our total free energy $F$. This model has been studied in the past close to a critical point by Leibler and Andelman [12]. In the present work we would like to extend the treatment to deep temperature quenches (far away from the critical region). Since the free energy functional $F$ depends at most only quadratically in the height profile $h(x, y)$, we can write it in Fourier space in terms of the $q$-modes of $\varphi$ and $h$: $\varphi_q$ and $h_q$, respectively

$$F_1 + F_3 = \int \left[ \frac{1}{2}(\sigma + \kappa q^2) q^2 h_q h_{-q} + \Lambda q^2 \varphi_q h_{-q} \right] \mathrm{d}\mathbf{q} \tag{2.4}$$

The degree of freedom $\{h_q\}$ can be traced out by performing a Gaussian integral $\int \mathcal{D}h_q \exp(-F/k_B T)$. Equivalently, we can find the same result (within mean field approximation) when the variation of $F$ with respect to $h_q$ is zero, $\delta F/\delta h_q = 0$. This condition yields a relation between $\varphi_q$ and $h_q$

$$h_q = -\frac{\Lambda}{\sigma + \kappa q^2}\varphi_q \tag{2.5}$$

Inserting $h_q$ from equation (2.5) into $F$ we obtain an effective free energy

$$F = \int \Big[-\frac{\Lambda^2}{2\kappa} + \frac{1}{2}bq^2 + \frac{\sigma}{2\kappa}\frac{\Lambda^2}{\sigma + \kappa q^2}\Big]\varphi_q\varphi_{-q}\,\mathrm{d}\mathbf{q} + \int \Big(f(\varphi) - \mu\varphi\Big)\mathrm{d}\mathbf{r} \tag{2.6}$$

The coefficient of the $\varphi_q\varphi_{-q}$ term has a $q$-independent contribution which merely shifts the critical temperature, the usual stiffness $q^2$ term and a third piece which goes to zero in the limit of large $q$. For low temperatures we are interested in the large $q$ limit of the kernel in equation (2.6), $\Gamma_q$

$$\Gamma_q = \frac{\sigma}{2\kappa}\frac{\Lambda^2}{\sigma + \kappa q^2} \tag{2.7}$$

Close to the lateral critical point, the small $q$-mode expansion can be justified as was investigated in the previous work [12]. Since here we will concentrate on sharp domain walls (for the A/B concentration profile) we are interested in the competition arising from the $\int \Gamma_q\varphi_q\varphi_{-q}\mathrm{d}\mathbf{q}$ term and the wall energy $\gamma$ associated with the change in the sharp change in A/B concentration. In position space the former can be written as:

$$F_{\mathrm{LR}} = \int \Gamma(x-y)\varphi(x)\varphi(y)\,\mathrm{d}y$$

$$= \frac{\Lambda^2}{4\xi\kappa}\int \mathrm{e}^{-|x-y|/\xi}\varphi(x)\varphi(y)\,\mathrm{d}y \tag{2.8a}$$

with a correlation length $\xi$ defined as

$$\xi = \Big(\frac{\kappa}{\sigma}\Big)^{1/2} \tag{2.8b}$$

where, for simplicity, we will consider in the remainder section, a two-dimensional system with a one-dimensional A/B concentration profile and interface. Hence, $\Gamma(x)$ is the exponentially decaying correlation function along the interface.

We would like to show that because of the coupling between curvature and composition, equation (2.8), a periodic arrangement of $n$ domains of A and $n$ domains of B has a lower free energy than just a fully segregated A/B system. If the domain size (of A and B) is $D$, then the energy cost for each domain wall in the system is $\gamma$. On the other hand, there is an energy gain resulting from equation (2.8). For a periodic arrangement of A and B domains, the integral in equation (2.8) can be performed exactly resulting in the following free energy density $f_{\mathrm{LR}} = F_{\mathrm{LR}}/2nD$,

$$f_{\mathrm{LR}} = \frac{\Omega}{D}\Big(\mathrm{e}^{-d} + d - 1\Big) - \frac{2\Omega}{D}\mathrm{e}^{-d/2}\sinh\frac{d}{2}\tanh\frac{d}{2}$$

and

$$\Omega \equiv \frac{\Lambda^2 \xi}{8\kappa}(\Delta\varphi)^2 \tag{2.9}$$

where $d \equiv D/\xi$. The first and second terms in equation (2.9) are the intra-domain and inter-domain contributions, respectively. The total free energy (per unit periodicity on the interface) is the sum of $f_{\mathrm{LR}}$ and the domain wall energy $\gamma/D$

$$f(D) = \frac{\gamma}{D} + f_{\mathrm{LR}} \tag{2.10}$$

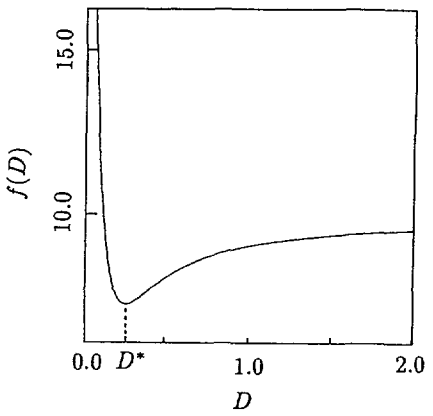


Fig. 1. — The free energy per unit length $f(D)$ as a function of the periodicity $D$. The competition between the domain wall energy and $f_{\mathrm{LR}}$ results in a minimum for $D = D^*$. The parameters chosen are $\gamma = 1.0$, $\Omega = 1.0$ and $\xi = 0.1$.

In figure 1, $f(D)$ is plotted for the following values of the parameters $\gamma = 1.0$, $\Omega = 1.0$ and $\xi = 0.1$. Indeed, one finds that the function $f(D)$ does have a single minimum at $D = 0.251$.

By taking the variation of $f(D)$ with respect to $D$, it is possible to see that $f(D)$ always has a minimum at $D = D^*$ satisfying

$$1 - \frac{\gamma}{\Omega} = (1+d)\mathrm{e}^{-d} + \left[-(d+2)\sinh\frac{d}{2} + d\cosh\frac{d}{2} + \frac{d}{\cosh(d/2)}\right]\mathrm{e}^{-d/2}\tanh\frac{d}{2} \tag{2.11}$$

Two cases can be distinguished: $d \ll 1$ and $d \gg 1$. In the former case, the correlation length $\xi$ is larger than the domain size $D$ and the inter-domain contribution to $f_{\mathrm{LR}}$ is important. The optimal domain size $D^*$ is obtained by expanding equation (2.11) to third order in $d$

$$D^* = \xi\left(\frac{6\gamma}{\Omega}\right)^{1/3} \tag{2.12}$$

Since $d$ is assume to be small, a consistency condition is that $\gamma/\Omega \ll 1$. If only the intra-domain contribution is taken in this case, the scaling law for $D^*$ is different: $D^* = \xi(\gamma/\Omega)^{1/2}$ instead of the more accurate result, equation (2.12).

In the other case of $d \gg 1$, the correlation length $\xi$ is small compared to the domain size $D$. A solution of equation (2.11) indicates that for this limit $\gamma/\Omega \simeq 1$ yielding an optimal domain size $D^*$

$$D^* = -\xi \log |1 - \frac{\gamma}{2\Omega}| \tag{2.13}$$

Again, a consistency check verifies that in this case $D^*/\xi \gg 1$ as long as the ratio $\gamma/2\Omega$ approaches one from below. Equation (2.11) can be investigated numerically for any value of $d$. An optimal finite periodicity $D^*$ minimizes the free energy $f(D)$ for any value of $D/\xi$ in between the two limiting behaviors presented above.

Since a periodic domain arrangement is chosen by the system due to the coupling between curvature and composition, it is also of interest to calculate how the shape profile $h(x)$ follows the composition profile $\varphi(x)$. We will consider only the symmetric case of A and B domains each of size $D$. Although the composition profile is always very sharp at low temperatures, the "sharpness" of the shape profile will depend on the correlation length $\xi$. Taking the inverse Fourier transform of equation (2.5) we obtain that the shape profile $h(x)$ is proportional to the convolution between the kernel $\Gamma(x)$ and the composition profile $\varphi(x)$:

$$h(x) = -\frac{\Lambda}{2\kappa}\xi \int_{-\infty}^{\infty} e^{-|x-y|/\xi}\varphi(y)\,dy \tag{2.14}$$

Taking $\varphi(x)$ as a periodic function alternating between two plateaus ($\varphi_A = \varphi_0$ for $2n < x/D < 2n+1$ and $\varphi_B = -\varphi_0$ for $2n+1 < x/D < 2n+2$), $h(x)$ can be calculated from equation (2.14)

$$h_A(x) = \Delta h\left[1 - \left(\frac{1}{1+e^{D/\xi}}\right)\left(e^{x/\xi} + e^{(D-x)/\xi}\right)\right] \tag{2.15a}$$

where

$$\Delta h \equiv -\frac{\Lambda}{2\kappa}\xi^2\Delta\varphi = -\frac{\Lambda}{2\sigma}\Delta\varphi \tag{2.15b}$$

and $\Delta\varphi = \varphi_A - \varphi_B = 2\varphi_0$.

As function of the size of the correlation length $\xi$ vs. the domain size $D$, the change in the shape profile $h(x)$ will be either gradual or abrupt. For $d = D/\xi \ll 1$, the shape does not follow the steps of the concentration profile. Rather, a smoothing effect here causes a parabolic shape profile extending all over the domain size $D$

$$h_A(x) = \frac{\Delta h}{2\xi^2}x(D-x) \tag{2.16}$$

Here the variation in the height profile is not $\Delta h$ as in the case $d \gg 1$ below, but rather a much smaller quantity $\Delta h d^2/8$ since $d \ll 1$ in this limit.

In the other case of $d = D/\xi \gg 1$, it is mainly the intra-domain contribution that counts. Here the variation in $h$, $\Delta h$ occurs on length scales of $\xi$ which is much smaller than the domain side $D$. Hence in this case, the shape follows quite closely the concentration profile. It alternates between two plateau values $h_A$ and $h_B$ and the variation is limited to a region of thickness $\xi$ around the domain wall.

$$h_A(x) = \Delta h\left(1 - e^{-x/\xi} - e^{(x-D)/\xi}\right) \tag{2.17}$$

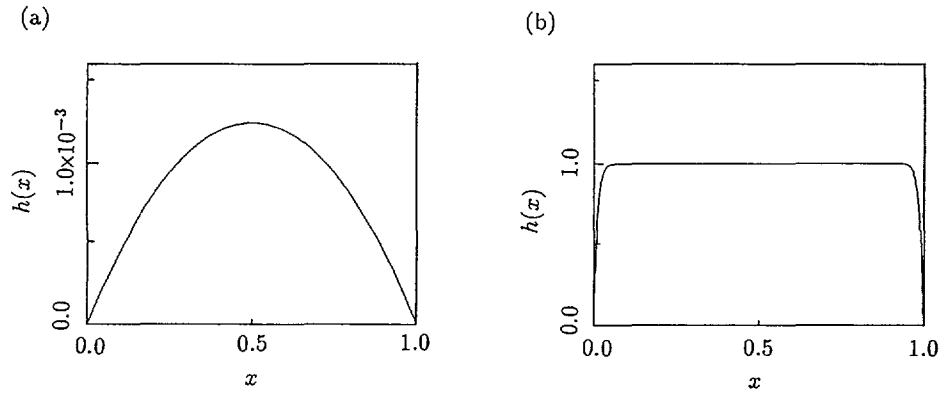


Fig. 2. — The shape profile $h(x)$ in an A domain for the case (a) $d \ll 1$ and the case (b) $d \gg 1$, respectively. Parameters used are $\Delta h = 1.0$, $D = 1.0$ and (a) $\xi = 10.0$ and (b) $\xi = 0.01$, respectively. The membrane shape is parabolic in case (a), while the membrane shape is almost flat except for sudden changes near the domain walls in case (b).

The two different limits can be understood physically in terms of the competition between the surface tension and curvature energies. Example of the membrane shape calculated from equation (2.15) for these two limits $d << 1$ and $d >> 1$ are shown in figures 2a and b, respectively. In the first case of large $\xi = \sqrt{\kappa/\sigma}$, the dominant energy is the curvature one. Here, the line length is not minimized but rather the system follows the curvature in each of the domains. In the other case, $\xi$ is small (compared with the domain size $D$). So here the surface tension is large and the system prefers to minimize the total line length by having a large portion of the domain which is flat and a steep height variation within an interval of size $\xi$ around the domain wall.

## 3. Cylindrical vesicles and vesicles in 2d space.

So far we have concentrated on almost planar membranes surrounded by a reservoir of amphiphilic molecules. In this section we turn our attention to closed-form vesicles and consider first vesicles with a cylindrical symmetry. The principal axis of the cylinder is assumed to extend to infinity (no end-caps) so the problem can be reduced to solving a two-dimensional (2d) problem of a closed one-dimensional (1d) contour defining the vesicle itself, enclosing an inner area of fluid. For clarity, we will refer in this section to a 1d vesicle embedded in a 2d space instead of talking of the cylindrical geometry. In addition, we will make the assumption that the total perimeter length of the vesicle is fixed, i.e., the amphiphilic layer which forms the vesicle is assumed to be an incompressible fluid layer. This means that not only the total perimeter length of the vesicle is constant but also the length of every line element on the perimeter is constant during the shape deformation, although the final results are the same whether we adopt the local incompressibility or the global incompressibility [23]. Actually, vesicles are incompressible to a large degree; namely, their area per amphiphile is fixed. In addition, processes such as exchanges of matter with monomers in solution, fission and fusion which change the overall size of the vesicle can be ignored if we consider only a single vesicle in thermodynamic equilibrium. Hence, our assumption of incompressibility of the line element on the perimeter is reasonable. Finally, we consider only *simply connected* vesicle shapes of

genus zero. In 2d this means that we look only at simply connected closed curves describing the vesicle perimeter.

**3.1** GENERAL FORMALISM. — For contours (vesicles) of fixed total length it is convenient to introduce a natural coordinate $s$, which is defined as the distance along the contour (known also as the chemical length) from a specified reference point on the contour (Fig. 3a). Let the *fixed* total length of the vesicle be $L$, then the parameter $s$ varies from 0 to $L$. Due to the fact that the vesicle has always a closed–shape form, a periodic boundary condition is required, i.e., $\mathbf{r}(L) = \mathbf{r}(0)$, where $\mathbf{r}(s) \equiv [x(s), y(s)]$ is the position vector of a point on the contour specified by $s$.

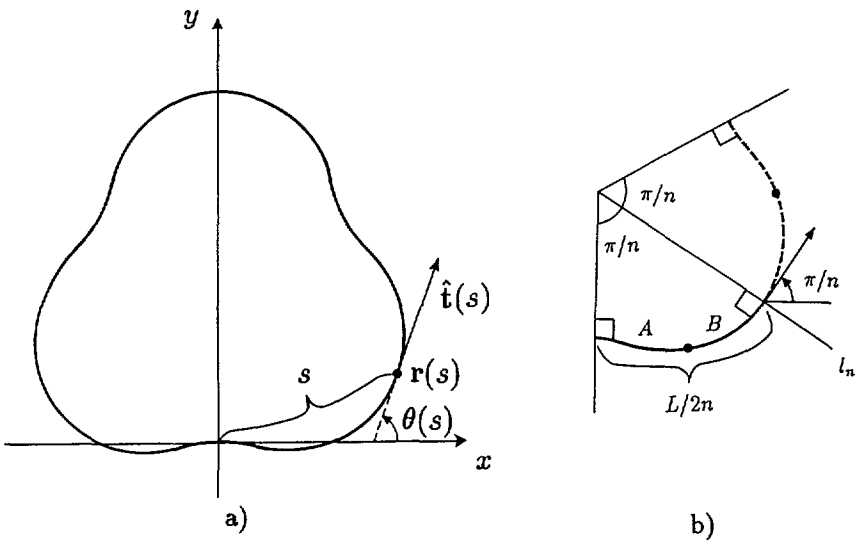


Fig. 3. — a) A schematic illustration of the model 1d membrane and parameters. b) An illustration of the closure condition for a vesicle in 2d space with an $n$-fold symmetry.

The total free energy functional $F$ discussed already in the previous section for the nearly flat membrane can now be expressed in terms of the natural parameter $s$

$$F = F_1 + F_2 + F_3 + \Delta P \cdot S\,,$$

and

$$F_1 = \int_0^L [\sigma + \frac{1}{2}\kappa c^2]\mathrm{d}s\,,$$

$$F_2 = \int_0^L \left[\frac{b}{2}\left(\frac{\mathrm{d}\varphi}{\mathrm{d}s}\right)^2 + f(\varphi) - \mu\varphi\right]\mathrm{d}s\,,$$

$$F_3 = \Lambda \int_0^L \varphi(s)c(s)\,\mathrm{d}s\,. \tag{3.1}$$

where $F_1$ describes the shape contribution, $F_2$ is the inplane free energy of mixing, $F_3$ is the coupling term and the last term of $F$ is a pressure term. The first three terms have been

introduced in the previous section and are expressed here in terms of $c(s)$, the local curvature of the vesicle at point $s$ as defined below. The fourth term is a new contribution specific to closed bodies. It is due to a possible pressure difference, $\Delta P$ across the vesicle, $\Delta P \equiv P_o - P_i$, where $P_o$ ($P_i$) is the pressure of the outer (inner) region, coupled to the inner area $S$ enclosed by the vesicle. Since the $\sigma$-term in $F_1$ [Eq. (3.1) ] is the surface tension term coupled to the over perimeter length, it can be omitted because the total perimeter length of the vesicle is taken to be constant. It will contribute only a constant to the free energy irrespective of the vesicle shape. In equation (3.1), we did not include the Gaussian curvature and the spontaneous curvature. In the present cylindrical vesicle case with a constant membrane area, the Gaussian curvature vanishes and the spontaneous curvature drops exactly since $\int_0^L c(s)\mathrm{d}s = 2\pi$.

Denoting the unit tangent vector of the contour at the point $s$ (Fig. 3a) as

$$\hat{\mathbf{t}}(s) = \frac{\mathrm{d}\mathbf{r}}{\mathrm{d}s} \equiv [\cos\theta(s), \sin\theta(s)] \tag{3.2}$$

where $\theta(s)$ is the angle between $\hat{\mathbf{t}}(s)$ and the $x$-axis. The curvature $c(s)$ and the total enclosed area $S$ can be expressed in terms of $s$:

$$c(s) = \left(\hat{\mathbf{t}} \times \frac{\mathrm{d}\hat{\mathbf{t}}}{\mathrm{d}s}\right)_z = \dot{\theta}(s) \tag{3.3}$$

and

$$S = \frac{1}{2}\int_0^L (\mathbf{r} \times \hat{\mathbf{t}})_z \, \mathrm{d}s = \frac{1}{2}\int_0^L [x(s)\sin\theta(s) - y(s)\cos\theta(s)]\mathrm{d}s \tag{3.4}$$

The dot operator in equation (3.3) means $\mathrm{d}/\mathrm{d}s$ and $(\cdots)_z$ means the $z$-component, where the $z$-axis is perpendicular to the plane containing the vesicle. Using these relations, equation (3.1) can be rewritten as:

$$F_1 = \frac{1}{2}\kappa \int_0^L \dot{\theta}^2(s)\,\mathrm{d}s$$

and

$$F_3 = \Lambda \int_0^L \varphi(s)\dot{\theta}(s)\,\mathrm{d}s \tag{3.5}$$

Moreover, since we limit our treatment to the strong segregation case of the A/B mixture, the expression for $F_2$, the free energy of inplane mixing, can be simplified as well. In this limit, the A/B mixture separates laterally into A-rich domains with $\varphi(s) = \varphi_A$ and B-rich domains with $\varphi(s) = \varphi_B$ bounded by sharp domain walls. Without loss of generality, we take the composition of the A and B domains to be $\varphi_A = \varphi_0$ and $\varphi_B = -\varphi_0$, respectively, since the free energy $F_2$ can be expressed as a symmetric form in the order parameter, $\varphi$ [24]. In addition, let us consider the simplified case where the vesicle is divided into $n$ domains of the A species and $n$ domains of the B species. In such a situation, apart from an irrelevant constant contribution, $F_2$ is merely

$$F_2 = 2n\gamma \tag{3.6}$$

where $\gamma$ is, as was introduced in the preceding section, the energy cost to produce *one* domain wall between an A and a B domain. Note that in 2d the sharp domain wall between A and B domain is a point defect. Unlike the surface tension $\sigma$ in equation (3.1) which is not relevant for vesicles of constant perimeter, $\gamma$ plays an important role.

The free energy $F$ given above has to be supplemented by the closure condition of the vesicle shape. From the definition of the unit tangent vector, equation (3.2), we find that

$$\mathbf{r}(s) = \mathbf{r}(0) + \int_0^s \hat{\mathbf{t}}(s')\mathrm{d}s' \tag{3.7}$$

Therefore, the closure condition can be written as:

$$\mathbf{r}(L) = \mathbf{r}(0) \quad \text{and} \quad \theta(L) = \theta(0) + 2\pi \tag{3.8}$$

As our shape equation (derived below from the free energy functional) is a second order differential equation, the closure condition requires continuity in $\mathbf{r}(s)$ and its first derivative $\dot{\mathbf{r}}(s) = \mathrm{d}\mathbf{r}(s)/\mathrm{d}s$ [25].

The equilibrium shape of the vesicle and the equilibrium amphiphile composition profile on the vesicle are obtained by *minimizing* the free energy functional $F$ with respect to $\theta(s)$ and the positions of $2n$ domain walls: $s_1, s_2, \ldots, s_{2n}$. In the strong segregation limit, the concentration of the amphiphile in the A and B domains is set to be $\varphi_0$ and $-\varphi_0$, respectively, and is independent of the vesicle shape. In addition, the ratio between the total line length of the A and B domains, $c_\mathrm{A}$, is also a constant. From equations (3.1) and (3.4-3.6), the minimization equations lead to:

$$\frac{\partial F}{\partial s_i} = 0 \qquad (i = 1, 2, \ldots, 2n)$$

and

$$\begin{aligned} \frac{\delta F}{\delta \theta(s)} &= -\kappa\ddot{\theta}(s) - \Lambda\dot{\varphi}(s) + \Delta P \cdot \frac{\delta S}{\delta\theta(s)} = 0 \\ \frac{\delta S}{\delta\theta(s)} &= \left[x(s) - \frac{1}{2}x(L)\right]\cos\theta(s) + \left[y(s) - \frac{1}{2}y(L)\right]\sin\theta(s) \end{aligned} \tag{3.9}$$

and $\dot{\varphi}(s)$ should be regarded as a set of $\delta$-functions located at every A/B domain wall since the domain wall width is always assumed to be the smallest length in the problem. In deriving equation (3.9), we used the assumption that the vesicle is composed of a locally incompressible fluid layer of amphiphilic molecules, which means that the perimeter length $s$ is an independent parameter of the vesicle shape. Equation (3.9) should be supplemented by the closure condition equation (3.8). One way of doing this is to introduce additional Lagrange multiplier terms in equation (3.9) in accord with the closure condition, equation (3.8).

Given the positions of the A/B domain walls, we can calculate the vesicle shape which minimizes the free energy $F$. For simplicity, we consider a symmetrical arrangement of $n$ A-domains ($\varphi = \varphi_0$) of length $L_\mathrm{A}/n$ and $n$ B-domains ($\varphi = -\varphi_0$) of length $L_\mathrm{B}/n$ each. Then the closure condition is greatly simplified to

$$\begin{aligned} &x(L/2) = 0 \quad \text{and} \quad y(L/2) = \text{arbitrary} \\ &\theta(0) = 0 \quad \text{and} \quad \theta(L/2) = \pi \end{aligned} \tag{3.10}$$

where we choose the point $s = 0$ on an axis of mirror symmetry [26] and took the $x$-direction to be parallel to the tangent vector $\hat{\mathbf{t}}(0)$. Therefore, the system has a mirror symmetry with respect to the $y$-axis [27]. Such a closure condition, equation (3.10), introduces an additional term of the form $\eta_x[x(L/2) - x(0)]$ into $F$, where $\eta_x$ is a Lagrange multiplier. As is seen from equation (3.10), there is no constraint for $y(L/2)$ because of the mirror symmetry, and no other

Lagrange multiplier for $y(L/2)$ is needed. Using equations (3.2) and (3.7), equation (3.9) is rewritten within each domain as:

$$\kappa\ddot{\theta}(s) + \eta_x \sin\theta(s) - \Delta P \cdot \frac{\delta S}{\delta\theta(s)} = 0 \tag{3.11}$$

The amount of the discontinuity in $\dot{\theta}$ entering at the $i$-th domain wall, $\Delta\dot{\theta}_i$, can be obtained by integrating equation (3.11) including the $\Lambda\dot{\varphi}(s)$ term within a small $s$ interval around the $i$-th domain wall:

$$\Delta\dot{\theta}_i = (-1)^{i+1}\frac{2\varphi_0\Lambda}{\kappa} \equiv (-1)^{i+1}\Delta\dot{\theta} \tag{3.12}$$

where the domain walls are numbered sequentially as $i = 1, 2, 3, \ldots, 2n$ and we use the convention that the zeroth domain (containing the $s = 0$ point) is an A-domain. Although the curvature changes discontinuously at every domain wall, $\theta(s)$ itself is continuous and the vesicle shape is still smooth at the domain wall.

The vesicle shape is obtained by adjusting $\dot{\theta}_0 \equiv \dot{\theta}(0)$ and $\eta_x$ in such a way that the solution of the set of equations (3.11) and (3.12) satisfies the closure condition equation (3.10). Such a solution can be obtained analytically for the special case of no imposed pressure difference, $\Delta P = 0$, and is detailed in the next section. For a general $\Delta P \neq 0$ we have to rely on a numerical calculation.

Finally, we would like to remark about the relation between our shape equation, equation (3.9), and shape equations derived by others [9, 19]. In fact, our shape equation resembles that of Seifert [9], while it looks differently than the one derived by Onuki [19]. Such differences originate from different definitions of the Lagrange multipliers which are related to the shape constraints. Although the Lagrange multipliers add extra terms to the shape equation, some of them cancel each other, resulting in the same final form as our equation (3.9). In fact, unlike what is stated in reference [19], it can be shown precisely that our shape equation and the one derived in reference [19] are equivalent, if the Lagrange multiplier terms are explicitly included in equation (3.9).

**3.2** VESICLE SHAPES WITHOUT IMPOSED PRESSURE DIFFERENCE. — When there is no imposed pressure difference, $\Delta P = 0$, equation (3.11) reduces to the well-known pendulum (Sine-Gordon) equation:

$$\kappa\ddot{\theta}(s) + \eta_x \sin\theta(s) = 0 \tag{3.13}$$

We separate the discussion about the solution of equation (3.13) into two cases: $n = 1$ and $n \geq 2$.

*The $n \geq 2$ case:* in this case one finds that the Lagrange multiplier $\eta_x$ vanishes for any $n \geq 2$. As is shown in figure 3b, the vesicle shape has a mirror symmetry with respect to the line $l_n$. The closure condition is satisfied simply by guaranteeing $\theta(L/2n) = \pi/n$. No constraint on $x(L/2n)$ is required and $\eta_x$ can be dropped. Using equation (3.12) we find

$$\dot{\theta}(s) \equiv \dot{\theta}_0 + \frac{1 + (-1)^{i+1}}{2}\Delta\dot{\theta} \tag{3.14}$$

in the $i$-th domain. The vesicle is composed of consecutive circular arcs with the curvature changing alternatively between two values, $\dot{\theta}_0$ and $\dot{\theta}_0 + \Delta\dot{\theta}$. Note that the elastic energy is distributed uniformly on the vesicle in this case. This can be confirmed by verifying that $\dot{\theta}(s) + (\Lambda/\kappa)\varphi(s) \equiv$ const. everywhere on the vesicle. Integrating equation (3.14) and substituting the result into equation (3.10), $\dot{\theta}_0$ is given by

$$\dot{\theta}_0 = \frac{2}{L}[\pi - \frac{\Delta\dot{\theta}}{2}(L - L_A)] = \frac{2}{L}[\pi - \frac{\Delta\dot{\theta}}{2}L_B] \tag{3.15}$$

where $L_A$ and $L_B$ are the total lengths of the A and B domains, respectively, and $L_A + L_B = L$. In figure 4, we show vesicle shapes for different numbers of domains: $n = 2, 3$ and 4 obtained for the case with equal volume fractions of the A and B species, i.e., $c_A \equiv L_A/L = L_A/(L_A+L_B) = 1/2$. The other parameters used are $L = \kappa = \varphi_0 = 1.0$ and $\Lambda = 10.0$ [See Sect. 3.4 below]. The vesicle shape is composed of consecutive circular arcs of alternating curvatures and the different segments are connected smoothly (no jump of the slope) at the boundary points. It is also interesting to note that the *bi-concave* shape for the $n = 2$ case somewhat resembles that of a red blood cell.

*The $n = 1$ case:* this is a special case of a vesicle that is fully phase separated into one single domain of A and of B each. In this case, the solution of equation (3.13) can be expressed by Jacobi elliptic functions (See Appendix A). The resulting vesicle shape is shown in figure 5, where the parameters are the same as those in figure 4. Each of the A and B domains is no longer an arc of constant curvature.

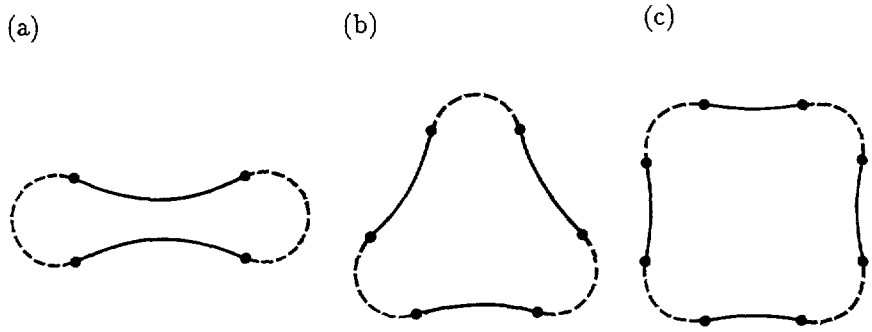


Fig. 4. — Vesicle shapes for $n = 2, 3$ and 4 with symmetric amphiphile composition, $c_A = 0.5$ under no imposed pressure difference, $\Delta P = 0$. The parameters are $L = \kappa = \varphi_0 = 1.0$ and $\Lambda = 10.0$. Solid and broken curves show A-domains ($\varphi_A = \varphi_0$) and B-domains ($\varphi_B = -\varphi_0$), respectively. For all $n$ values the vesicle shape is composed of consecutive circular arcs.

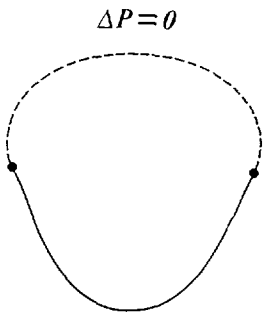


Fig. 5. — Vesicle shape for $n$=1 case. The parameters are the same as those used in figure 4. The vesicle shape is not composed of circular arcs.

The above discussion for vesicle shapes can be extended for any volume fraction of the A and B domains and not only for the case with equal volume fractions of the two species. In figure 6, we show vesicle shapes for various values of $c_A$, the A/B ratio, while keeping all other parameters as those used in figure 4. As apparent from figure 6 and in accord with our general discussion, for any value of $c_A$, the vesicle is composed of consecutive arcs (with constant curvature) for $n \geq 2$.

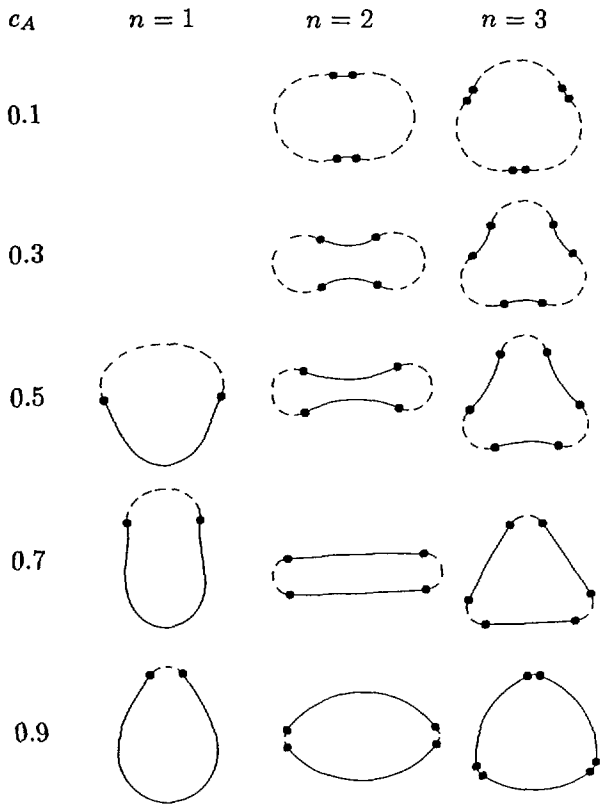


Fig. 6. — Same as figures 4 and 5 but for various values of the composition. Vesicle shapes are also expressed by consecutive circular arcs for $n \geq 2$. For $n = 1$, the vesicle shapes cannot be calculated for $c_A \leq 0.3$ as is explained in Appendix A.

In order to determine the most stable shape configuration of the vesicle under the assumption of an $n$-fold symmetry, one has to evaluate the free energy $F$ for each of the shapes. Using equations (3.5), (3.14) and (3.15), we obtain for $n \geq 2$

$$F_1 = 2\kappa\left(\pi^2 + \frac{1}{4}(\Delta\dot{\theta})^2 c_A(1-c_A)\right)$$

and

$$F_3 = 2\Lambda\varphi_0\left[\pi(2c_A - 1) - \Delta\dot{\theta}c_A(1-c_A)\right] \tag{3.16}$$

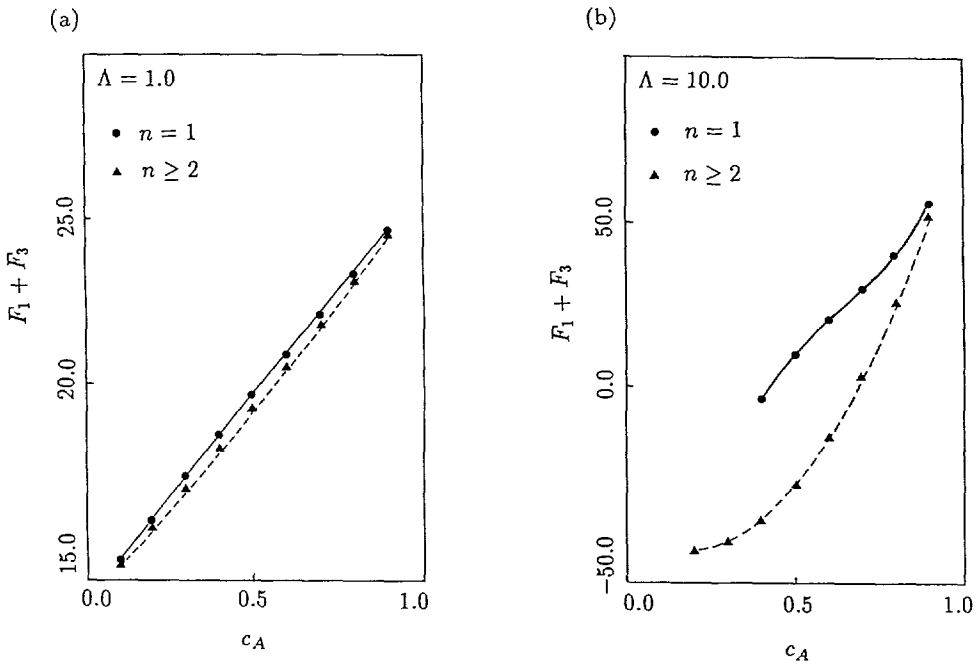


Fig. 7. — Comparison of the free energy $F_1+F_3$ between $n = 1$ and $n \geq 2$ cases for various amphiphile compositions. The parameters used are $\Lambda = 1.0$ in (a), and $\Lambda = 10.0$ in (b). In both cases, $L = \kappa = \varphi_0 = 1.0$ and $\Delta P = 0$. For $n \geq 2$, analytical expressions for $F_1, F_2$ and $F_3$ are given in equations (3.6) and (3.16). For $n = 1$ we rely on a numerical solution. Vesicle shape for $n = 1$ and $c_A \leq 0.3$ cannot be calculated because of the same reasons as those appearing in figure 6.

Both $F_1$ and $F_3$ do not depend on $n$ for $n \geq 2$. $F_2 = 2n\gamma$ as in equation (3.6) the total free energy $F = F_1 + F_2 + F_3$ is found to be a monotonically increasing function of $n$ for $n \geq 2$.

In figure 7, we compare the free energy $F_1 + F_3$ for $n \geq 2$ as appears in equation (3.16) with the one for $n = 1$ which was evaluated numerically, as function of the amphiphile composition ratio, $c_A$, and for $\Lambda = 1.0$ and 10.0. Due to the non-uniform curvature of the vesicle in the $n = 1$ case, $F_1 + F_3$ is always the largest for $n = 1$ than that of any $n \geq 2$. Therefore, the most stable configuration with a minimum total free energy $F = F_1 + F_2 + F_3$ is either $n = 1$ or $n = 2$. Defining $\Delta F_{13}$ as difference of $F_1 + F_3$ between the $n = 1$ and $n = 2$ cases, $\Delta F_{13} \equiv (F_1 + F_3)_{n=1} - (F_1 + F_3)_{n=2}$, then the $n = 1$ configuration is the most stable, if twice of the domain wall energy, $2\gamma$, is larger than $\Delta F_{13}$. On the other hand, if $2\gamma$ is smaller than $\Delta F_{13}$, the $n = 2$ configuration is most stable.

**3.3** VESICLE SHAPES WITH IMPOSED PRESSURE DIFFERENCE: $\Delta P \neq 0$. — Up to now the pressure difference $\Delta P$ across the vesicle, introduced in equation (3.1), was assumed to be zero. If $\Delta P$ is non-zero, we have to solve equation (3.11) taking the $\Delta P \cdot \delta S/\delta\theta(s)$ term into account. Thus, for any given value for $\Delta P$, the equilibrium vesicle shape is obtained by solving equation (3.11) numerically under the condition equation (3.10). More details about the solution are presented in appendix A. In figures 8 and 9, we show the vesicle shape calculated for $n = 2$ and $n = 4$, respectively. The pressure difference $\Delta P$ is negative in part (a), zero in (b) and positive in (c). Part (b) of these figures corresponds to the case of no pressure

difference, $\Delta P = 0$, discussed in the previous section. Whereas the vesicle shape is composed of consecutive arc-like segments when $\Delta P = 0$ [part (b)], each segment of the vesicle deviates from an arc-like shape and the curvature changes even within a single domain when $\Delta P \neq 0$ [parts (a) and (c)]. As the pressure difference $\Delta P \equiv P_o - P_i$ becomes more and more negative (the pressure increases from inside), the vesicle shape swells and approaches a circular shape in the limit of $\Delta P \to -\infty$. On the other hand, if $\Delta P$ becomes large (an increased external pressure), the vesicle shape becomes squashed until a point is reached when different segments of the vesicle start to touch each other. At this point our scheme for evaluating the vesicle shape breaks down because we do not take into account the interaction between distant segments of the vesicle.

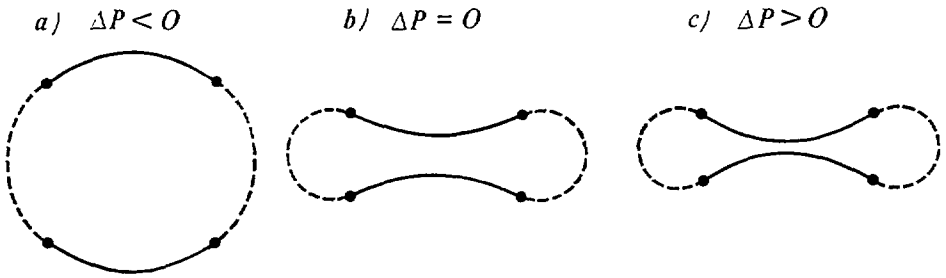


Fig. 8. — Vesicle shapes for $n = 2$ under imposed pressure difference $\Delta P$: (a) $\Delta P = -1.0 \times 10^4$, (b) $\Delta P = 0$ and (c) $\Delta P = 3.0 \times 10^2$. The other parameters are: $L = \kappa = \varphi_0 = 1.0$, $c_A = 0.5$ and $\Lambda = 10.0$.

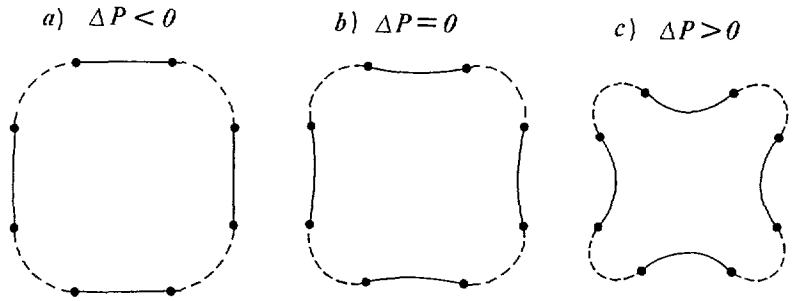


Fig. 9. — Same as figure 8 but for $n = 4$. (a) $\Delta P = -5.0 \times 10^3$, (b) $\Delta P = 0$ and (c) $\Delta P = 5.0 \times 10^3$. The other parameters are as in figure 8.

**3.4** PHASE DIAGRAMS FOR VESCILES IN 2d SPACE. — In order to obtain the phase diagram for closed-shape vesicles, the free energy functional $F$ defined by equation (3.1) is evaluated numerically for $n = 1, 2, 3, ..$ Comparing the different solutions, the most stable $n$-mode which has the minimum free energy $F$ is found.

Four independent and dimensionless parameters can be identified by rescaling distances by $L$ and energies by $\kappa/L$:

$$\tilde{\gamma} \equiv (L/\kappa)\gamma, \quad \tilde{\Lambda} \equiv (L\varphi_0/\kappa)\Lambda, \quad \Delta\tilde{P} \equiv (L^3/\kappa)\Delta P \quad \text{and} \quad c_A \equiv \frac{L_A}{L} = \frac{L - L_B}{L} \tag{3.17}$$

According to these scaling properties it is enough to consider the case $L = \kappa = \varphi_0 = 1.0$ without loss of generality.

The overall feature of the phase diagram can be understood by looking at the qualitative behavior of $F_1 + F_3$ and $F_1 + F_3 + \Delta P \cdot S$ for various values of $\Lambda$, $\Delta P$ and $n$. Numerical evaluations show that the quantity $F_1 + F_3$ is almost constant for any $n \geq 2$ within numerical error even under a nonzero imposed pressure difference, $\Delta P$, and a nonzero coupling, $\Lambda$ [28]. The $n = 1$ case is special, where $F_1 + F_3$ has a larger value than that for $n \geq 2$ as was shown in the preceding section.

On the other hand, $F_1 + F_3 + \Delta P \cdot S$ changes as $n$ changes even for $n \geq 2$ due to the $n$-dependence of the enclosed area $S$. In figure 10, the $n$ dependence of $F_1 + F_3 + \Delta P \cdot S$ is shown for a value of the coupling constant, $\Lambda = 10.0$, and for various values of $\Delta P$. This figure and the above argument show that the change in $F_1 + F_3 + \Delta P \cdot S$ is dominated by the changes in the enclosed area $S$. Note that $F_1 + F_3 + \Delta P \cdot S$ is a monotonically increasing (decreasing) function of $n$ when $\Delta P$ is positive (negative) except for $n = 1$. As the total free energy $F$ is the sum of this function and $F_2 = 2n\gamma$, we deduce that the $n = 2$ mode is the most stable one from all the $n \geq 2$ modes when $\Delta P$ is positive. Therefore, when $\Delta P$ is negative, the most stable mode depends on the value of the domain wall energy $\gamma$ as will be discussed below.

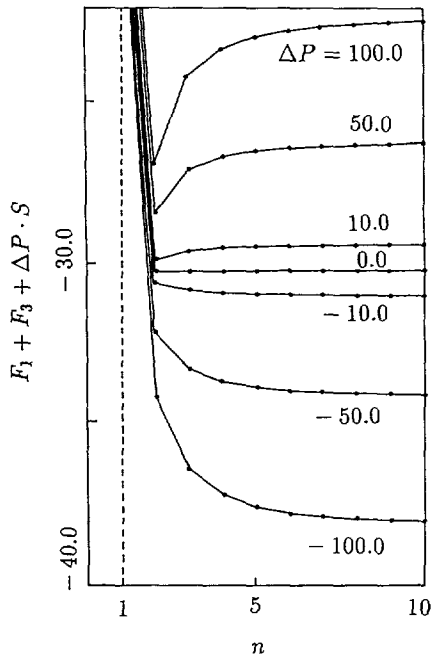


Fig. 10. — $F_1 + F_3 + \Delta P \cdot S$ as a function of the $n$ mode for $\Lambda = 10.0$ ($L = \kappa = \varphi_0 = 1.0$). From top to bottom, $\Delta P$ = 100.0, 50.0, 10.0, 0, -10.0, -50.0 and -100.0.

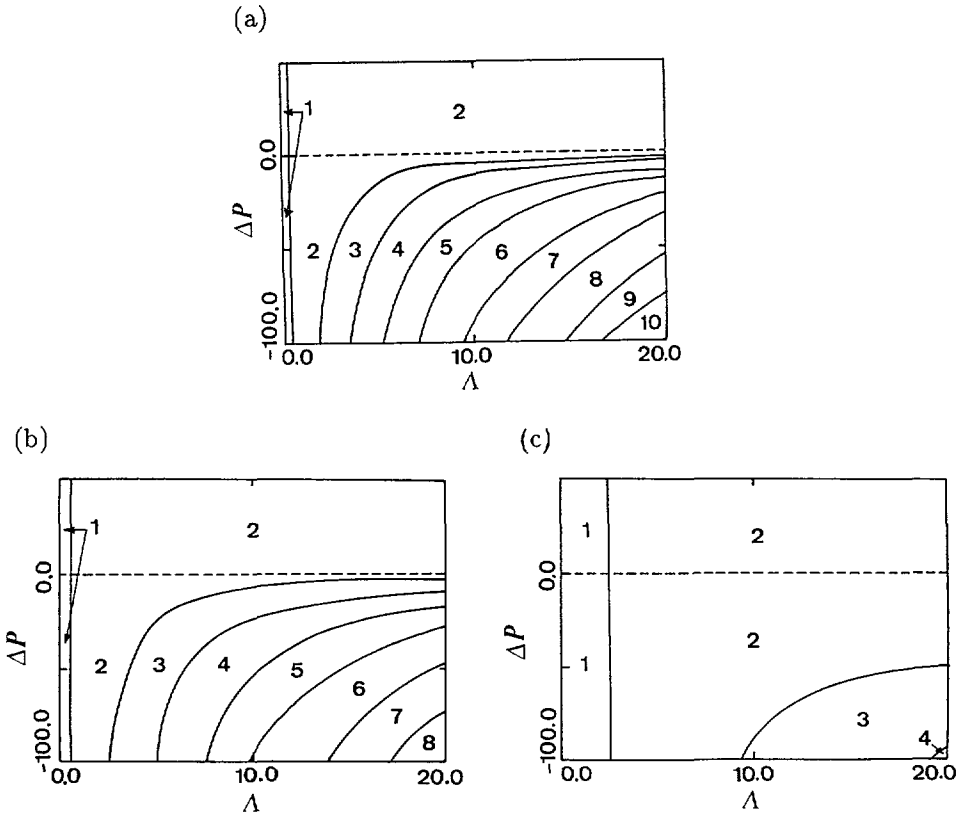


Fig. 11. — Phase diagrams (stability diagrams) for (a) $\gamma = 0.05$, (b) $\gamma = 0.1$ and (c) $\gamma = 1.0$ ($L = \kappa = \varphi_0 = 1.0$). The numbers in the figure indicate the values of $n$.

The case of $\Lambda = 0$ (no coupling) should be considered separately. In this case the vesicle shape is a perfect circle [29] irrespective of the mode, $n$, of the phase separation because there is no coupling between the vesicle shape and inplane phase separation. This means that the value of $F_1 + F_3 + \Delta P \cdot S$ is just the same as that of a one-component vesicle, which is independent of the mode $n$ of the phase separation. Therefore, the most stable mode for $\Lambda = 0$ is determined by minimizing $F_2$ and leads to the most stable mode $n = 1$ with just two domain walls separating the A and B domain.

In figure 11 we plot the stability diagram showing the most stable mode $n$ with the minimum free energy for several values of $\gamma$. The values of $\gamma$ are (a) 0.05, (b) 0.1 and (c) 1.0, respectively. As was mentioned above, the $n = 2$ mode is the most stable one when $\Delta P \geq 0$ except in the vicinity of the $\Lambda = 0$ (no coupling) line. When $\Delta P < 0$, and as a function of $\Lambda$, higher modes with $n > 2$ become the most stable ones. This behavior can be easily understood in the following way.

The difference in the total free energy $F$ between states with different mode numbers $n$ is determined only by the enclosed area $S$ and the domain wall energy $\gamma$. When $\Delta P < 0$, a larger enclosed area is preferred because the inner pressure is greater than the outer one. In order to obtain a larger enclosed area, a higher $n$ mode is selected because such a higher mode has a shape which is closer to the asymptotic circular shape. This tendency competes with the

domain wall energy $F_2 = 2n\gamma$ which imposes a penalty for higher $n$ modes, and the vesicle hence selects a finite value of $n$.

In figure 11, one finds that higher and higher $n$-modes are selected as the pressure difference $\Delta P$ becomes more negative while keeping $\Lambda$ and $\gamma$ constant. This is because the pressure term in the above competition becomes more and more dominant as $\Delta P$ becomes negative. An opposite situation takes place when $\gamma$ is increased while keeping $\Delta P(< 0)$ and $\Lambda$ constant. In this case, the contribution from the domain wall energy $2n\gamma$ increases, which imposes a larger penalty to a higher mode $n$ and the most stable mode is decreased (see Figs. 11a–c).

On the other hand, when the coupling $\Lambda$ becomes larger while keeping $\Delta P(< 0)$ and $\gamma$ constant, the vesicle shape deviates more and more from a circular shape. This leads to an increase in the $S \cdot \Delta P$ term because $\Delta P < 0$. The system prefers a higher $n$-mode in order to compensate such an energy loss. It is worth noting that the overall features of the phase diagrams for the strong segregation case shown in figure 11 are very similar to those for the weak segregation case [14, 20].

## 4. Vesicles in 3d space: axially symmetric case.

Our results for vesicles in 2d space can be extended to vesicles embedded in a three-dimensional (3d) space. Treating the general shape of 3d vesicles is extremely difficult. Usually it is done by choosing a convenient parametrization and an expansion for shapes that have small deviation from spheres, planes, cylinders, etc. However, if we restrict the treatment to include only 3d vesicles with a uniaxial symmetry (body of revolution), the parametrization of the surface is quite simple and the problem reduces to an effective 2d problem. As in the 2d case, we will assume that the vesicle area is conserved. Namely, the number of amphiphile and the area per amphiphile on the surface remain fixed.

The free energy functional, then, is very similar to that of the 2d system, equation (3.1)

$$F = F_1 + F_2 + F_3 + \Delta P \cdot V$$

and

$$F_1 = \int \left[\sigma + \frac{1}{2}\kappa c_{\mathrm{m}}^2\right] \mathrm{da}$$

$$F_2 = \int \left[\frac{b}{2}\left(\frac{\mathrm{d}\varphi}{\mathrm{d}s}\right)^2 + f(\varphi) - \mu\varphi\right] \mathrm{da}$$

$$F_3 = \Lambda \int \varphi(s) c_{\mathrm{m}} \, \mathrm{da} \tag{4.1}$$

where $c_{\mathrm{m}}$ is the mean curvature, da is the area element on the vesicle, and $\Delta P$ the pressure difference coupled to the inner volume $V$ enclosed by the vesicle. Although we do not allow *area* changes of the vesicle, changes of the *enclosed volume* are allowed. In this 3d case, we can no longer assume the symmetry in the $\varphi$-field ($\varphi \to -\varphi$) as was done in the 2d case. A constant shift in $\varphi$ causes an extra spontaneous curvature which cannot be eliminated for 3d vesicles because $\int c_{\mathrm{m}} \mathrm{da}$ is no longer a constant. Moreover, it is not possible, in general, to neglect the spontaneous curvature term in equation (4.1).

Nevertheless, for simplicity, we consider here only the A/B symmetric case. Namely, $\varphi_{\mathrm{A}} = \varphi_0$ and $\varphi_{\mathrm{B}} = -\varphi_0$ and setting the spontaneous curvature to zero. In the strong segregation limit, $F_2$ is estimated to be $l \cdot \gamma_{3\mathrm{d}}$ where $l$ is the sum of all the domain wall lengths, and $\gamma_{3\mathrm{d}}$ is the domain wall energy per unit length.

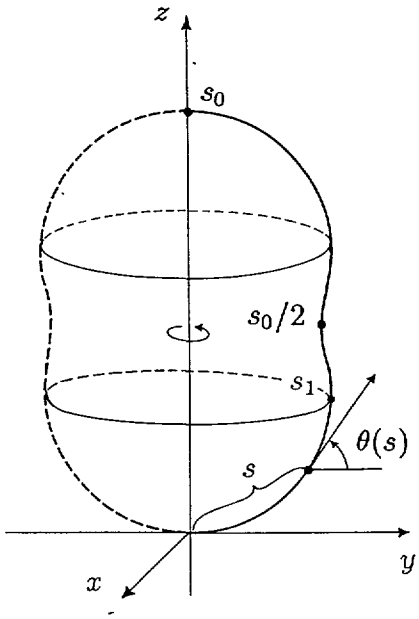


Fig. 12. — An illustration of a vesicle embedded in 3d space with uniaxial symmetry.

Here, again the Gauss-Bonnet Theorem tells us that the Gaussian curvature does not enter into equation (4.1) as long as the topology of a closed simply-connected (genus zero) shape is conserved [30]. Moreover, we can also disregard the $\sigma$ term in equation (4.1) (as was done in 2d), because the total area of the vesicle surface is kept constant.

As we assumed uniaxial symmetry, the shape and the free energy can be expressed in a similar way as was done for the 2d case in the preceding sections. The vesicle is described by the contour of its cross-section that contains the axis of symmetry. Introducing the $x$ and $y$ axes and the angle variable $\theta(s)$ as is shown in figure 12, the mean curvature $c_{\mathrm{m}}$ is given by [5]

$$c_{\mathrm{m}} = \frac{1}{2}\Big(\dot{\theta}(s) + \frac{\sin\theta(s)}{x(s)}\Big) \tag{4.2}$$

where the axis of symmetry is taken as the $z$-axis and the coordinate $s$ is the distance from a reference point $(x, z) = (0, 0)$ on the contour. Here, the total contour length is no longer a constant, because the contour is merely the *cross-section* of a 3d body of revolution. It is only the 2d *area* of the vesicle which is fixed. Equation (4.1) can be rewritten using the relation $\mathrm{d}a = 2\pi x(s)\mathrm{d}s$ and equation (4.2)

$$F_1 = \frac{\pi\kappa}{4}\int_0^{s_0}\Big(\dot{\theta}(s) + \frac{\sin\theta(s)}{x(s)}\Big)^2 x(s)\,\mathrm{d}s$$

and

$$F_3 = \pi\Lambda\int_0^{s_0}\Big(\dot{\theta}(s) + \frac{\sin\theta(s)}{x(s)}\Big)x(s)\varphi(s)\,\mathrm{d}s \tag{4.3}$$

where the $\sigma$ term is dropped in $F_1$ and $2s_0$ is the perimeter length of the cross-section to be determined from the closure condition of the contour and the fixed area condition. The total

vesicle surface area $S_M$ is given by

$$S_M = 2\pi \int_0^{s_0} x(s)\,ds \equiv \text{const.} \tag{4.4a}$$

where $S_M$ is constrained to some constant value. The inner volume enclosed by the vesicle, $V$, is given by

$$V = \pi \int_0^{s_0} x^2(s)\,\sin\theta(s)\,ds \tag{4.4b}$$

Moreover, in this 3d case, we have to take the conservation of the order parameter $\varphi$ into account explicitly:

$$\int \varphi(\mathbf{a})da = \varphi_0(S_A - S_B) \tag{4.4c}$$

where $S_A$ and $S_B$ are the total areas of A and B domains satisfying $S_A + S_B = S_M$, respectively. This condition can be rewritten in the present uniaxial case as:

$$2\pi \int_0^{s_0} x(s)\varphi(s)\,ds = \varphi_0(S_A - S_B) \tag{4.4d}$$

Using equations (4.1), (4.3) and (4.4a - 4.4d), we see that only the following free energy functional has to be considered:

$$\hat{F} = \frac{\pi\kappa}{4} \int_0^{s_0} x(s)\Big(\dot{\theta}(s) + \frac{\sin\theta(s)}{x(s)} + \frac{2\Lambda}{\kappa}\varphi(s)\Big)^2 ds + 2\pi\gamma_{3d} \sum_i x(s_i) \quad + \quad \Delta P \cdot V \tag{4.5}$$

where the first term equals to $F_1 + F_3$ and the second term comes from the domain wall energy $F_2$. The difference between the free energies, $F$ and $\hat{F}$, is an irrelevant contribution $\int(\Lambda^2/\kappa^2)x(s)\phi^2(s)ds$, which has the same form as equation (4.4a) since $\varphi^2(s) = \varphi_0^2 = \text{const.}$, and thus can be adsorbed into $S_M$.

On the surface of a 3d vesicle, a domain wall separating A and B domains is a 1d line. However, for the simple case of a body of revolution, the domain wall is characterized by its coordinate $s_i$ on the contour (see Fig. 12). In equation (4.5), we did not introduce any Lagrange multiplier associated with the constant vesicle area condition, equation (4.4a), or the conservation law for the $\varphi$-field equation (4.4d), because such constraints can be satisfied by adjusting the parameter $s_0$ and the positions of the domain boundaries. When a deformation of the vesicle shape takes place, the total length of domain walls changes even if the total amphiphile composition is kept constant. Therefore, we have to include contributions from $F_2$ in equation (4.5), in contrast to the 2d case where only the number of domain walls $n$ entered into the free energy. The equilibrium contour equation is given by the variational principle of $\hat{F}$ with respect to $\theta(s)$

$$\begin{aligned}\frac{\delta\hat{F}}{\delta\theta(s)} = 0 = &-\frac{\pi\kappa}{4}\sin\theta(s)\int_s^{s_0}\Big[\Big(\dot{\theta}(s') + \frac{2\Lambda}{\kappa}\varphi(s')\Big)^2 - \Big(\frac{\sin\theta(s')}{x(s')}\Big)^2\Big]\,ds' - \\ &-\frac{\pi\kappa}{2}x(s)\frac{d}{ds}\Big(\dot{\theta}(s) + \frac{2\Lambda}{\kappa}\varphi(s) + \frac{\sin\theta(s)}{x(s)}\Big) - \\ &-2\pi\,\gamma_{3d}\,\sin\theta(s)\sum_i H(s_i - s) \quad + \quad \Delta P \cdot \frac{\delta V}{\delta\theta(s)}\end{aligned} \tag{4.6}$$

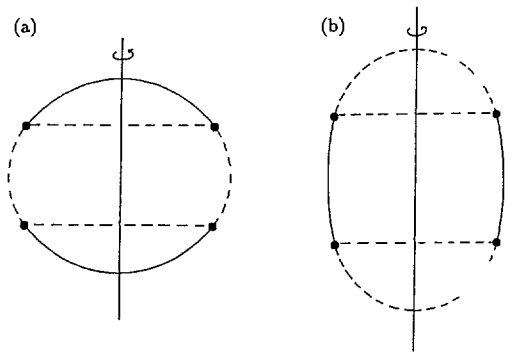


Fig. 13. — Cross-section of vesicles with uniaxial symmetry are shown for (a) an A-B-A configuration and (b) a B-A-B configuration. The parameters used are $\kappa = \varphi_0 = S_M = 1.0$, $\Lambda = 0.5$, $\Delta P = \gamma_{3d} = 0$ and $c_A = 0.5$.

where $H(x)$ is the Heavyside function defined as $H(x) = 1$ for $x \geq 0$ and $H(x) = 0$ for $x < 0$. The explicit expression for $\delta V/\delta\theta(s)$ is given by

$$\frac{\delta V}{\delta\theta(s)} = \pi x^2(s)\cos\theta(s) - 2\pi\sin\theta(s)\int_s^{s_0} x(s')\sin\theta(s')\,ds' \tag{4.7}$$

The discontinuity in $\dot{\theta}$ at every domain boundary in 3d is given by integrating equation (4.6) as

$$\Delta\dot{\theta}_i = 2(-1)^{i+1}\Delta\dot{\theta} \tag{4.8}$$

which is different from equation (3.12) by a factor 2 due to the difference in the dimensionality. In solving equations (4.6) and (4.8), we have to adjust $\dot{\theta}(0)$, $s_0$ and the positions of domain boundaries $s_1, s_2, \ldots$, under the closure condition at $s = s_0$.

For simplicity, we present here the case where the vesicle has a mirror symmetry about a plane perpendicular to the axis of uniaxial symmetry and with the parameters $\gamma_{3d} = \Delta P = 0$. In such a case the closure condition is just $\theta(s_0/2) = \pi/2$, whereas the values of $x(s_0/2)$ and $y(s_0/2)$ remain arbitrary. Then, the equilibrium condition is obtained from equation (4.6) as

$$\sin\theta(s)\int_s^{s_0/2}\left[\left(\dot{\theta}(s') + \frac{2\Lambda}{\kappa}\varphi(s')\right)^2 - \left(\frac{\sin\theta(s')}{x(s')}\right)^2\right]ds'$$

$$+\ 2x(s)\frac{d}{ds}\left[\dot{\theta}(s) + \frac{2\Lambda}{\kappa}\varphi(s) + \frac{\sin\theta(s)}{x(s)}\right] = 0 \tag{4.9}$$

subjected to conditions, equations (4.4a) and (4.4d).

Note that equation (4.9) does not allow a solution when the bending energy is distributed uniformly on the vesicle even in the case $\Delta P = 0$. One can easily confirm this by assuming

$$\dot{\theta}(s) + \frac{2\Lambda}{\kappa}\varphi(s) + \frac{\sin\theta(s)}{x(s)} = C \tag{4.10}$$

where $\kappa C^2/8$ is a measure of the bending energy per unit area on the vesicle [31], assumed to be a constant throughout the vesicle. For further details see appendix B (and the discussion above Eq. (3.15) for the 2d case).

Table I. — *Comparison between the free energy of the A-B-A and the B-A-B configurations shown in figure 13. Parameters are* $\Lambda = 0.5$, $\kappa = \varphi_0 = S_M = 1.0$, $\Delta P = 0$, $\gamma_{3d} = 0$ *and* $c_A = 0.5$.

| type | | $F_1$ | $F_3$ | $F_1 + F_3$ | $l$ |
|---|---|---|---|---|---|
| (a) | A-B-A | 6.41 | −0.23 | 6.18 | 3.18 |
| (b) | B-A-B | 6.76 | −0.37 | 6.39 | 2.77 |

Two simple cases of symmetrical domain arrangement are considered: A-B-A (a B domain in between two A's) and inversely B-A-B. More details are given in Appendix C. In figure 13, we give examples of the cross-sections of the vesicles for (a) an A-B-A configuration and for (b) a B-A-B configuration. Vertical lines show the axis of uniaxial symmetry. Parameters used are $\kappa = \varphi_0 = S_M = 1.0$, $c_A \equiv S_A/S_M = 0.5$ and $\Lambda = 0.5$ in both (a) and (b), while keeping always $\gamma_{3d} = \Delta P = 0$. As the A (B) domains tend to be less (more) convex towards the outer side, the vesicle is elongated in the direction perpendicular to the axis in case (a) and in the direction parallel to the axis in case (b). In table I, we give a comparison of the free energy values of these two vesicles. The A-B-A configuration has the lower free energy but has the larger domain wall length $l$ than those of the B-A-B configuration. Therefore, the A-B-A configuration is more stable than the B-A-B configuration when the domain wall energy is small. When the domain wall energy becomes larger, the B-A-B configuration will be selected. This conclusion is valid as long as we neglect the change in the vesicle shape imposed by a non-zero domain wall energy $\gamma_{3d}$. When the domain wall energy is large enough, it can dominate the shape deformation and can induce budding of the membrane [17, 18].

## 5. Conclusion.

Two-component membranes and vesicles can undergo an appreciable shape deformation through a coupling between spontaneous curvature and the local composition of the two-component amphiphiles. We find that two-component (A/B) membranes and vesicles show periodic domain structure in two situations: (a) unilamellar membranes with both surface tension and curvature; and (b) closed shape vesicles subjected to an external pressure (osmotic pressure).

In the former case, the membrane is assumed to be in equilibrium with the surrounding reservoir of the amphiphilic molecules, dictating a surface tension. Previous studies have been carried out close to the critical temperature [11, 12], while here we look at the strongly segregated A/B mixture. The intrinsic domain periodicity of the membrane may correspond to a particular example of a ripple phase of the membrane. This periodicity is determined by the competition between the A/B domain wall energy ($\gamma$) and the energy which arises from the local coupling between the concentration and curvature of the different domains. The shape of the membrane is shown to be quite different in two limiting cases: when the domain size $D$ is smaller than the correlation length, $\xi = \sqrt{\kappa/\sigma}$, (e.g., large bending modulus) the membrane shape profile is piece-wise parabolic with a small out-of-plane amplitude around the flat reference plane. In the other case of small bending modulus, $D$ much bigger than $\xi$, the membrane shape has sharp height variations at the domain boundaries. The variation occurs over a short length scale of order $\xi$. Hence, here the membrane shape follows almost precisely the steps of the concentration profile.

In addition to unilamellar membranes, we treated also the case of closed shape vesicles. To a

good approximation their perimeter can be considered as constant so their energetics depends entirely on curvature and not on surface tension. An intrinsic wave number is found only when there is an imposed pressure difference (osmotic pressure) across the vesicle. In this case, the intrinsic wave number arises from the competition between the domain wall energy and the work done by the vesicle against the imposed pressure difference. Our formalism is easily extended to uniaxial vesicles (body of revolution) in 3d space, where we find that the domain wall energy plays an important role in determining the equilibrium shape deformations.

We would like to comment about the relation between this work and several other recent papers. Whereas we concentrated here on two-component membranes and vesicles in the two-phase region (temperatures below the critical one), Seifert [16] investigated a similar two-component membrane problem but in the homogeneous one-phase region (temperature is above the critical temperature). In his case, the problem can be mapped into an effective one-component problem as long as the system does not approach the phase separation region. This cannot be done in our case of a segregated system below $T_c$. We note as well that the importance of the domain wall energy on the shape deformation has also been addressed by Lipowsky and Jülicher [17, 18] in connection with *budding* phenomena of vesicles.

Other interesting directions of research are investigations of shape deformations of membranes coupled to a vector field on the membrane [15] or a study of the dynamics, where the phase separation process is affected by the geometrical changes of the membrane shape [19]. Another possible extension is to try to include singular (cusp-like) domain walls as is expected in the ripple phase [10]. Although at present we assumed that the vesicle shape is smooth at the domain walls, such a singular nature may be incorporated into our model.

Finally, we performed similar investigations also for the weak segregation case, and the results will be given in the accompanying paper [20].

**Acknowledgements.**

We would like to thank M. E. Fisher, F. Jülicher, D. Lichtenberg, R. Lipowsky, H. Müller-Krumbhaar, A. Onuki, V. Pokrovsky, S. Safran and W. Zimmermann for discussions and comments. This work started while one of us (D.A.) was visiting Kyushu University. He would like to thank the Yamada Foundation for a travel fellowship. Partial financial support from the Israel Academy of Sciences and Humanities and the German Israel Binational Foundation (G.I.F) under grant No. I-0197 is gratefully acknowledged. T.K. and K.K. thank the Yamada Foundation, Alexander von Humboldt Stiftung and IFF KFA Jülich, for the financial support during their stay in Germany. Computation was performed at the Computer Center of the Institute for Molecular Science, Japan. This work is also supported by the Scientific Research Fund of the Ministry of Education, Science and Culture, Japan.

## Appendix A. Technical details for 2d vesicles

In this appendix, we present a detailed procedure to calculate numerically the vesicle shape for 2d closed-shape vesicles with $n$-fold symmetry. Unlike the $n \geq 2$ case, where $\eta_x$ vanishes and the vesicle shape is obtained analytically, for the $n = 1$ case we have to rely on numerical calculations to solve equation (3.13). The Lagrange multiplier $\eta_x$ no longer vanishes on symmetry grounds, since it is impossible to connect smoothly two semi-circles of different curvatures (no change in the slope) at the two joining points. Thus, we have to solve equation (3.13) with appropriate non-zero values of $\eta_x$ and $\dot{\theta}_0$. The solution of equation (3.13) can be expressed by the Jacobi elliptic functions, and $\eta_x$ and $\dot{\theta}_0$ are found numerically by an iteration method that

ensures the closure condition equation (3.10). Such an iteration procedure does not always converge and sometimes we cannot get the solution for the shape. For example, we could not find any solutions for $c_A \leq 0.3$ (Fig. 6). When we approach $c_A \sim 0.3$, the convergence of the iteration scheme fails to converge for reasons which are not entirely understood at the moment.

When the vesicle is subjected to a non-vanishing imposed pressure difference, $\Delta P \neq 0$, the shape evaluation is always numerical and is different for $n \geq 2$ and for $n = 1$. First, we discuss the $n \geq 2$ case. As the vesicle has an $n$-fold symmetry, the third equation of equation (3.9) and equation (3.11) can be rewritten in such a way that $L \longrightarrow L/2$ in equation (3.9) and an extra factor of 2 in front of $\Delta P$ in the *l.h.s.* of equation (3.11) due to the mirror symmetry. Using the $n$-fold symmetry, equation (3.10), we find that $x(L/2)$ vanishes and $y(L/2)$ can be combined with the Lagrange multiplier $\eta_x$ yielding

$$\kappa\ddot{\theta}(s) + \eta_x \sin\theta(s) = \Delta P\,[x(s)\cos\theta(s) + y(s)\sin\theta(s)] \tag{A.1}$$

Integrating equation (A.1) with respect to $s$ over the interval $[0, L/n]$ and using $x(0) = y(0) = 0$, we arrive at

$$\kappa[\dot{\theta}(L/n) - \dot{\theta}(0) - (\Delta\dot{\theta}_1 + \Delta\dot{\theta}_2)] + \eta_x y(L/n) = \frac{\Delta P}{2}[x^2(L/n) + y^2(L/n)] \tag{A.2}$$

where $\Delta\dot{\theta}_i$ is the discontinuous change in the slope $\dot{\theta}(s)$ at the $i$-th domain boundary, equation (3.12). Since $\dot{\theta}(L/n) = \dot{\theta}(0)$ from the $n$-fold symmetry and $\Delta\dot{\theta}_1 + \Delta\dot{\theta}_2 = 0$, we obtain

$$x^2(L/n) + \Big(y(L/n) - \frac{\eta_x}{\Delta P}\Big)^2 \quad = \quad \Big(\frac{\eta_x}{\Delta P}\Big)^2 \tag{A.3}$$

which states that the points $\Big(x(iL/n),\, y(iL/n)\Big)$, $i = 1, \ldots, n$, are on a circle of radius $\eta_x/\Delta P$ centered at $(0, \eta_x/\Delta P)$. Another way of writing equation (A.3) is

$$\frac{2\eta_x}{\Delta P} \quad = \quad \frac{x^2(L/n) + y^2(L/n)}{y(L/n)} \tag{A.4}$$

Substituting equation (A.4) back into equation (A.1), yields

$$\kappa\ddot{\theta}(s) \quad = \quad \Delta P\Big\{x(s)\cos\theta(s) + \Big[y(s) - \frac{x^2(L/n) + y^2(L/n)}{2y(L/n)}\Big]\sin\theta(s)\Big\} \tag{A.5}$$

For a given $\Delta P$, we have to determine $\dot{\theta}(0)$, $x(L/n)$ and $y(L/n)$ self-consistently under the closure conditions $\theta(L/n) = 2\pi/n$. This can be done by the following procedure. First we select a trial value for $\dot{\theta}(0)$. Using such a value of $\dot{\theta}(0)$, one can solve equation (A.5) where the values of $x(L/n)$ and $y(L/n)$ are determined by an iteration procedure. The value of $\dot{\theta}(0)$ is adjusted till the iteration procedure converged to a closed–shape vesicle with smoothly joining boundaries.

The above procedure cannot be applied to the $n$=1 case. Although equations (A.1-A.4) are still valid, we cannot use equation (A.5) because we obtain $y(L/n) = y(L) = 0$ in $n = 1$. The appropriate iteration procedure can be obtained by integrating equation (A.1) *twice* with respect to $s$:

$$\eta_x \int_0^{L/2} y(s)\mathrm{d}s \;-\; \frac{\Delta P}{2}\int_0^{L/2}[x^2(s) + y^2(s)]\mathrm{d}s$$
$$+\kappa\Big(\pi - [\dot{\theta}(0) + \Delta\dot{\theta}_1]\frac{L}{2} + \Delta\dot{\theta}_1 s_1\Big) \;=\; 0 \tag{A.6}$$

where we used the closure condition $\theta(L/2) = \pi$. This equation can be used as an iteration relation for $\eta_x$ instead of equation (A.4).

## Appendix B. Nonuniformity of the bending energy for 3d vesicles

In this appendix we show that the assumption of uniform distribution of the bending energy, equation (4.10), conflicts with the equilibrium condition equation (4.9), in 3d.

Substituting equation (4.10) into equation (4.9) leads to

$$\int_s^{s_0/2} C\Big[\dot{\theta}(s') + \frac{2\Lambda}{\kappa}\varphi(s') - \frac{\sin\theta(s')}{x(s')}\Big]\,\mathrm{d}s' = 0 \tag{B.1}$$

which should hold for any value of $s$. Thus,

$$\dot{\theta}(s) + \frac{2\Lambda}{\kappa}\varphi(s) - \frac{\sin\theta(s)}{x(s)} = 0 \tag{B.2}$$

From equations (4.10) and (B.2), we obtain

$$\dot{\theta}(s) = \frac{1}{2}[C - \frac{4\Lambda}{\kappa}\varphi(s)] \tag{B.3}$$

As $\varphi(s)$ takes a constant value ($\varphi_0$ or $-\varphi_0$) within the interval $s \in [0, s_1]$ and $\theta(0) = 0$, we see that $\theta(s)$ from equation (B.3) is proportional to $s$, and

$$\theta(s) \equiv \alpha s = \frac{1}{2}(C \mp \frac{4\Lambda}{\kappa}\varphi_0)s \qquad \text{for} \qquad s \in [0, s_1] \tag{B.4}$$

where $\alpha$ is a constant whose value is found using equations (3.2) and (3.7)

$$\alpha = \frac{\sin\theta(s)}{x(s)} = \frac{\sin\alpha s}{\int_0^s \cos\alpha s'\,\mathrm{d}s'} \qquad \text{for} \qquad s \in [0, s_1] \tag{B.5}$$

One can easily confirm that equations (B.4) and (B.5) are compatible with equation (B.2) only if $\Lambda = 0$ (or equivalently if $\varphi_0 = 0$).

## Appendix C. Technical details for 3d vesicles

Here, we describe how to solve equation (4.9). Defining

$$\psi(s) = \frac{\sin\theta(s)}{x(s)}$$

$$f(s) = \int_0^s \Big[\Big(\dot{\theta}(s') + \frac{2\Lambda}{\kappa}\varphi(s')\Big)^2 - \psi^2(s')\Big]\,\mathrm{d}s'$$

and

$$A = f(s_0/2) \tag{C.1}$$

Keeping in mind that the $\varphi(s)$ term is constant within a single domain, it can be dropped out and equation (4.9) can be rewritten as

$$\frac{\mathrm{d}}{\mathrm{d}s}\Big(\dot{\theta}(s) + \psi(s)\Big) + \frac{1}{2}\psi(s)\Big(A - f(s)\Big) = 0 \tag{C.2}$$

We solve equation (C.2) using the initial condition, $\theta(0) = 0$, $\dot{\theta}(0) = \dot{\theta}_0$, $\psi(0) = \dot{\theta}_0$ and $f(s) = 0$, where $\dot{\theta}_0$ is the curvature at $s = 0$ to be determined. In order to solve equation (C.2) we employ an iteration method to obtain $A$ in a self-consistent manner and also to adjust $\dot{\theta}_0$, $s_0$ and $s_1$ to the conditions equations (4.4a) and (4.4d).

Extra attention should be paid to the singularity at $s$=0. The evolution equation for the variable $\psi(s)$

$$\frac{\mathrm{d}}{\mathrm{d}s}\psi(s) = \frac{\cos\theta}{x^2}\Big(x\dot{\theta} - \sin\theta\Big) \tag{C.3}$$

appears to have a singularity at $s$=0 where $x(s)$ vanishes. However, expanding the *r.h.s.* of equation (C.3) in a Taylor series in $s$ and using equation (4.9), we obtain

$$\lim_{s\to 0}\frac{\mathrm{d}}{\mathrm{d}s}\psi(s) = \frac{1}{2}\ddot{\theta}(0) = -\frac{1}{6}\dot{\theta}_0 A \tag{C.4}$$

which has a finite limiting value.

## References


[1] Physics of Complex and Supermolecular Fluids, S. A. Safran and N. Clark Eds., (Wiley, New York, 1987).

[2] Physics of Amphiphilic Layers, D. Langevin, J. Meunier and N. Boccara Eds., (Springer, Berlin, 1987).

[3] Modern Ideas and Problems in Amphiphilic Sciences, W. M. Gelbart, D. Roux and A. Ben-Shaul Eds., to be published.

[4] Helfrich W., *Z. Naturforsch.* **28c** (1973) 693.

[5] Deuling H. J. and Helfrich W., *Biophys. J.* **16** (1976) 861.

[6] Helfrich W., *Z. Naturforsch* **33a** (1978) 305.

[7] Ostrowsky N. and Peyraud J., *J. Chem. Phys.* **77** (1982) 2081.

[8] Leibler S. and Maggs A., *Phys. Rev. Lett.* **63** (1989) 406.

[9] Seifert U., *Phys. Rev. A* **43** (1991) 6803.

[10] Gebhardt C., Gruler H. and Sackmann E., *Z. Naturforsch.* **32c** (1977) 581.
Sackmann E., *Biomembranes* **5**, D. Chapmann Ed. (Academic Press, New-York, N.Y., 1985).

[11] Leibler S., *J. Phys. France* **41** (1986) 109.

[12] Leibler S. and Andelman D., *J. Phys. France* **48** (1987) 2013.

[13] Andelman D., Kawakatsu T. and Kawasaki K., *Europhys. Lett.* **19** (1992) 57.

[14] Taniguchi T., Kawasaki K., Andelman D. and Kawakatsu T., *Cond. Matt. Materials Commun.* in press.

[15] MacKintosh F. C. and Lubensky T. C., *Phys. Rev. Lett.* **67** (1991) 1169.

[16] Seifert U., *Phys. Rev. Lett.* **70** (1993) 1335.

[17] Lipowsky R., *J. Phys. II France* **2** (1992) 1825.

[18] Jülicher F. and Lipowsky R., *Phys. Rev. Lett* **70** (1993) 2964.

[19] Onuki A., *J. Phys. Soc. Jpn* **62** (1993) 385.

[20] Taniguchi T., *et al.*, in preparation.

[21] Coxeter H. S. M., Introduction to Geometry (J. Wiley, New York, 1965).

[22] Safran S. A., Pincus P. and Andelman D., *Science* **248** (1990) 354.
Safran S. A., Pincus P. A., Andelman D. and MacKintosh F. C., *Phys. Rev. A* **43** (1991) 1071.

[23] Jenkins J. T., *J. Math. Biol.* **4** (1977) 149;
Zhong-can O.-Y. and Helfrich W., *Phys. Rev. Lett.* **59** (1987) 2486.

[24] The assumption of symmetric equilibrium values of the $\varphi$-field does not impose any restrictions on our model in 2d. If $\varphi_A \neq \varphi_B$, one can redefine $\varphi$ by $\varphi - (\varphi_A + \varphi_B)/2$. Since $\int_0^L \dot{\theta}(s)\,ds = 2\pi$, one can easily confirm that the extra terms arising from this transformation give only constant contributions to the free energy.

[25] The origin $s = 0$ should not coincide with any of the domain boundaries because we assumed continuity conditions at $s = 0$ and $s = L$.

[26] There always exists at least one axis of mirror symmetry for any $n \geq 1$.

[27] The continuity condition for $\dot{\theta}(s) \equiv d\theta(s)/ds$ at $s = 0$ is automatically satisfied under equation (3.10) due to the mirror symmetry.

[28] We do not believe that $F_1 + F_3$ is exactly constant in such situations, but the actual deviation from a constant is numerically very small. For the case of $\Delta P = 0$, one can confirm from equation (3.16) that $F_1 + F_3$ is actually constant. When $\Delta P \neq 0$, such a property can be obtained only numerically.

[29] If the outer pressure difference $\Delta P$ becomes larger than a certain critical value, a perfectly circular shape is no longer stable and the vesicle undergoes a large deformation like a biconcave red blood cell. In this paper, we totally neglect such possibilities. However, if $\Lambda = 0$, the phase separation is independent of the shape and the most stable mode is $n = 1$. [See Seifert U., Berndl K. and Lipowsky R., *Phys. Rev. A* **44** (1991) 1182.].

[30] The Gauss-Bonnet Theorem still holds for our two component vesicles although the Gaussian curvature changes discontinuously at every domain wall. (We assumed same Gaussian bending moduli for both domains). As the vesicle shape itself is smooth (not cusp-like), the Gaussian curvature does not diverge but only changes discontinuously at the domain walls. Therefore, the contribution from such a discontinuity to the elastic energy is negligible because the width of the domain wall region is taken to be smaller than any other length in the problem in the strong segregation limit.

[31] One can confirm this from equation (4.3), which leads to:

$$F_1 + F_3 = \frac{\pi\kappa}{4} \int_0^{s_0} x(s) \left( \dot{\theta}(s) + \frac{\sin\theta(s)}{x(s)} + \frac{2\Lambda}{\kappa}\varphi(s) \right)^2 + \text{const.}$$

$$= \frac{\kappa}{8} S_M C^2 + \text{const.}$$